ISEIS

Journal of Environmental Informatics 43(2) 118-128 (2024)

Journal of Environmental Informatics

www.iseis.org/jei

Sediment Grain Size Affects Vegetation Patterns in River-Dominated Deltas

L. Zhi[1, 2 *], X. Xie[1 *], W. Gao[1, 3, 4], X. Li[1 **], J. Bai[1 **], D. Wang[1], D. Shao[1], and B. Cui[1]

[1] *State Key Laboratory of Water Environment Simulation, School of Environment, Beijing Normal University, Beijing 100875, China*
[2] *School of Earth Science and Engineering, Hebei University of Engineering, Handan 056038, China*
[3] *Research and Development Center for Watershed Environmental Eco-Engineering, Advanced Institute of Natural Science, Beijing Normal University at Zhuhai, Zhuhai 519087, China*
[4] *Yellow River Estuary Wetland Ecosystem Observation and Research Station, Ministry of Education, Dongying 257500, China*

Received 15 April 2022; revised 11 September 2023; accepted 12 September 2023; published online 15 April 2024

ABSTRACT. River deltas contain some of the most densely populated areas in the world and are characterized by a rich biodiversity and highly productive ecosystems. Although previous studies have revealed that sediment grain size plays a key role in determining delta morphology, its subsequent effects on deltaic vegetation distribution patterns remain elusive. We used a theoretical templet to facilitate our study by conducting numerical experiments to simulate deltaic morphological evolution in response to various sediment grain sizes and explored the vegetation distribution determined by the elevation profile of a typical river-dominated delta. Our results showed that a fine-grained, cohesive delta would develop vegetation patterns transitioning from high- to low-elevation adapted vegetation species with increasing distance, whereas the same vegetation transformation trend could occur with decreasing distance to the center of a large-grained, noncohesive delta. The modeled vegetation distribution pattern of fine-grained, cohesive and large-grained, noncohesive deltas could be well demonstrated in the natural deltas. In addition, vegetation distribution patterns are related to the grain size-driven morphological processes of deltas, and the leading role of cohesive and noncohesive sediments on constructed delta is critical in determining the resulting vegetation distribution pattern. The dominance of each vegetation type would gradually become stable as delta matures. The interspecies competitions could influence distribution patterns of each vegetation type by enhancing the fragmentation of mid-elevation adapted vegetation. The effects of sediment grain size on the deltaic vegetation patterns associated with a delta's morphological processes have potential implications for the conservation and restoration of deltaic habitats.

Keywords: river-dominated delta, sediment grain size, deltaic morphology, vegetation distribution pattern

1. Introduction

River deltas provide a variety of biodiversity, enormous ecosystem services and socioeconomic benefits (Barbier et al., 2011; Liviu et al., 2014). However, river deltas have been threatened by intensive anthropogenic activities such as land reclamation and sea level rise driven by global climate change, which have resulted in the degradation of deltaic ecosystems and loss of vegetation habitats (Ma et al., 2019; Nienhuis et al., 2020). To facilitate delta management and restoration, it is urgent to better understand the ecological structures of deltas, particularly regarding their vegetation distribution patterns. Generally, a delta's ecological structure is determined by its morphologic evolution processes (Paola et al., 2011; Liviu et al., 2014). Previous researches have addressed the key role of sediment grain size in driving delta morphology (Edmonds et al., 2010; Geleynse et al., 2011; Caldwell et al., 2014). However, it is still unclear how delta morphology transformations caused by varied sediment grain sizes impact the vegetation distribution patterns of deltas.

Generally, delta morphology is controlled by the interplay between river discharge, tides, and waves (Galloway, 1975; Nienhuis et al., 2020), and deltas can exhibit different morphological features with similar fluvial regimes and marine energy levels under varied grain sizes (Syvitski and Saito, 2007). In addition, Geleynse et al. (2011) showed that the delta morphology would be controlled by surface sediment composition in a similar way in the presence of both waves and tides. Numerical modeling has revealed that the sediment settling velocities and critical shear stresses for erosion together control delta-building processes (e.g., mouth bar growth, bifurcation, avulsion and levee growth) (Lauzon et al., 2018; Gao et al., 2019), and result in shifts in delta morphology from an elongated shape with stable sinuous channels to a semicircular shape with many ephemeral channels (Edmonds and Slingerland, 2010; Caldwell and Edmonds, 2014). However, although previous researches have discussed the effects of grain size on delta morphology, vegetation distribution pattern on a delta shaped by sedimentary grain size still remains unclear.

Within deltaic systems, environmental conditions are driv-

* Co-first authors.
** Corresponding author. Tel.: +86 010-58806857.
E-mail address: lixw@bnu.edu.cn (X. Li).
** Corresponding author. Tel.: +86 010-58802029
E-mail address: junhongbai@163.com (J. Bai).

ISSN: 1726-2135 print/1684-8799 online
© 2024 ISEIS All rights reserved. doi:10.3808/jei.202400514.

en by riverine and marine processes, such as river currents, sedimentation, tides and storms (Paola et al., 2011). Due to the low surface elevation gradient of deltas, their abiotic factors are generally sensitive to and determined by deltaic landforms, and thus, different types of vegetation preferably inhabit various elevation zones (Bertness et al., 1987; Wilcox, 2004). For example, in a fully developed river-dominated delta, woody plants are dominant in the highest elevation zones, abundant grasses and forbs can be found in intermediate elevation zones, and submerged aquatic vegetation (e.g., seagrass) thrives in the lowest inundated elevation zones (Wilcox, 2004; White et al., 2016).

River-derived sediment is critical in shaping deltaic landforms and further controls the vegetation composition and zonation, as well as its diversity (Carle et al., 2015; Larsen, 2019; Twilley et al., 2019). Recent studies have revealed that the river floods and sediment yields delivered into a delta could change its vegetation distribution pattern by modifying the deltaic landform (Rosen et al., 2013; Ma et al., 2018). River floods and high sediment concentrations promote both the horizontal and vertical growth of a delta and accelerate transformations in its vegetation distribution and community composition (Carle et al., 2015). Although vegetation-based processes and patterns in river deltas have been well documented (Wilcox, 2004; Rosen and Xu, 2013; Carle et al., 2014), how vegetation patterns are driven by altered delta morphologies due to varied sediment grain sizes still needs to be further explored.

To fill this gap, our research, therefore, focused on exploring the general formation mechanism of a templet-based river-dominated estuarine ecosystem with varied sediment grain size driven by hydro-morphological processes coupling with vegetation dynamics, in addressing following specific objectives: (1) to compare hydro-morphological and vegetation patterns of a river-dominated delta shaped by varied sediment grain size and (2) to understand how sediment grain size influence and determine different vegetation patterns on a river-dominated delta.

To conduct research, we established a templet-based river-dominated delta and employed the numerical models to simulate the vegetation distribution processes following deltaic morphological evolution with different sediment grain sizes. As a river-dominated and sediment-rich estuarine ecosystem facilitates tidal vegetation development and provides multiple ecological functions such as endangered waterbird habitats, natural coastal defense, blue carbon sequestration, and water purification, our research therefore has potential general implications for ecological management and manipulation of hydrological flow and sediment control to promote conservation and rehabilitation for a river-dominated estuarine ecosystem.

2. Methods

2.1. Morphodynamic Model Set Up

Delft3D is a physics-based model that simulates water flow and sediment transportation and is commonly used in studies on estuarine-deltaic morphological evolution (Edmonds and Slingerland, 2010; Geleynse et al., 2010; Geleynse et al., 2011; Caldwell and Edmonds, 2014; Gao et al., 2018, 2019). In this research, we used a 2D depth-averaged morphodynamic model following the setup in Edmonds and Slingerland (2010), for a hypothetical river-dominated delta. This 2D model was generally used in modeling delta morphology and had been approved that the modeled deltas are representative of real deltas by comparing the discharge ratios between bifurcate channels, bed heights of the bifurcate arms scale and flood maps in field observation (Syvitski and Saito, 2007; Edmonds and Slingerland, 2010; Geleynse et al., 2010; Caldwell and Edmonds, 2014; Gao et al., 2018). The computational domain is with 300 × 225 rectangle computational cells (25 × 25 m resolution), and the Chezy coefficient is defined as having a constant value of 45 $m^{1/2}/s$ (Figure 1) (Edmonds and Slingerland, 2010; Caldwell and Edmonds, 2014). The initial depth of the receiving basin increases seaward with a milder initial basin slope of 0.000683. The morphological evolution in river-dominated delta was mainly controlled by flow hydrodynamics. The effects of waves and tides were not considered in our model to minimize the disturbance to the deposition process of cohesive sediment in the delta and thus highlighted its impacts on relevant morphodynamic processes in river-dominated deltas (Edmonds and Slingerland, 2010; Caldwell and Edmonds, 2014).

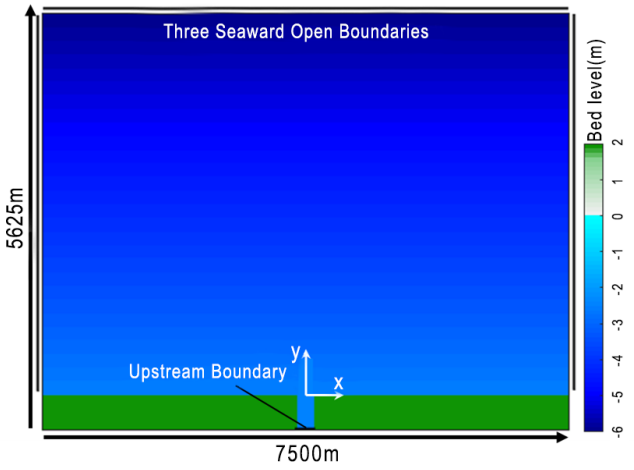

Figure 1. Computational domain and open boundaries in the Delft3D model in the research.

In Delft3D, the sediments were defined as cohesive sediments ($D50 \leq 64$ μm) or noncohesive sediments ($D50 > 64$ μm) by median diameter (Deltares, 2013). Cohesive sediment transportation was modeled according to a depth-averaged advection-diffusion formula (Partheniades, 1965). The settling velocities of the cohesive sediments were defined by Stoke's law, and the salinity affecting sediment flocculation was ignored. The erosion and deposition processes of cohesive sediment were considered following the Krone - Mehta - Partheniades formulations (Partheniades, 1965), and the value of criti-

cal shear stress for the erosion and deposition of cohesive sediments was set to be the same as that defined by Caldwell and Edmonds (2014). Noncohesive sediment transportation was computed according to the method described by Van Rijn (1993), while the transportation direction affected by local flow conditions and bed slopes was considered and referred to the Bagnold-Ikeda expressions (Ikeda, 1982).

The model had four open boundaries, including one upstream river boundary and three seaward boundaries (Figure 1). At the upstream river boundary, constant river discharge enters the receiving basin at one initial river channel defined as being 2.5 m deep and 250 m wide (Figure 1). Three seaward open boundaries were prescribed with a constant water surface elevation equal to zero (Figure 1) (Edmonds and Slingerland, 2010). To reach fully developed hydrodynamic and sediment transport conditions, a spin-up time of 720 min was used in every scenario before morphological evolution was allowed. The time step of the model was set as 12 s to ensure modeling accuracy and stability. The morphological scale factor was set as 60 to accelerate the morphological evolution. The sensitivity analysis was conducted with user-defined model parameters, such as varied time steps and morphological scale factors. The delta area, shape and vegetation pattern exhibited minimal differences when changing those parameters. The key modeling parameters are listed in Table 1.

Table 1. The Key Parameters in Modeling

Modeling parameters	Value	Units
Grid size	300 × 225	cells
Cell size	25 × 25	m
Initial sediment layer thickness at bed	10	m
Time step	12	s
Chezy coefficient	45	$m^{1/2}$ s^{-1}
Background horizontal eddy viscosity and diffusivity	0.0001	m^2 s^{-1}
Cohesive sediment critical shear stress for erosion	1	N/m^2
Cohesive sediment critical shear stress for deposition	1000	N/m^2
Morphological scale factor	60	-
Spin-up interval before morphological updating begins	720	min

In this study, we set five grain size variation scenarios (S1 ~ S5) (Table 2). The diameter of sediments was chosen ranging from cohesive sediments to noncohesive sediment to present the different delta morphologies with varied sediment grain sizes. In the cohesive scenarios (S1 ~ S2), the sediments were composed of a cohesive sediment fraction with a concentration (*COH*) of 0.2 kg/m^3 and a noncohesive sediment fraction (D_{50}: 200 μm). In the noncohesive scenarios (S3 ~ S5), a uniform sediment grain size with an equilibrated sediment concentration was prescribed at the upstream river boundary. River discharge also impacts delta morphology (Shaw et al., 2014; Bevington et al., 2017). In this study, we assumed that the river discharge remained constant. This assumption assumes that the delta mainly undergoes significant geomorphological evolution during flood season and the geomorphic effect during the low runoff period could be ignored to improve the simulation efficiency (Edmonds et al., 2007; Caldwell and Edmonds, 2014). For the various grain size scenarios (S1 ~ S5), five morphological years were defined to simulate fully developed deltas, assuming that the river experiences 30 days of bankfull conditions per year. These scenarios therefore can represent approximately 60 years of changes in delta morphology, which is already long enough for the development of the spatial patterns of deltaic vegetation.

Under natural conditions, sediments are generally composed of a variety of different components in a delta. Therefore, this study set up a series of proportional gradient scenarios of cohesive to noncohesive sediment ratios (%Co), the %Co is the percentage of cohesive sediment in the total sediment volume coming into the calculation domain at the end of the simulation. Four additional scenarios (S6 ~ S9) were created by changing the cohesive sediment concentration based on scenario S1 and ran until the same amount of sediment was delivered to the computational domain.

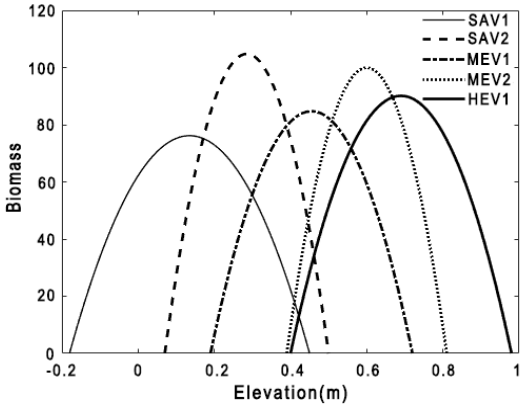

Figure 2. The biomass-elevation curves of the different vegetation types. SAV is submerged aquatic vegetation, MEV is mid-elevation vegetation and HEV is high-elevation vegetation.

2.2. The Simulation of Vegetation Distribution Patterns

As elevation is considered the key factor impacting the spatial distribution of vegetation species (Paola et al., 2011; Ning et al., 2021), we used a site-based elevation pattern to simulate the vegetation distribution on the delta. Considering elevation-based vegetation zonation, three vegetation classes were defined, including high-elevation vegetation (HEV) (e.g., woody species), mid-elevation vegetation (MEV) (e.g., tidal herbaceous species), and submerged aquatic vegetation (SAV). Each class included two typical vegetation types (Table 3). Then, we quantified the relationship between the vegetation biomass and elevation of each vegetation type by using the equation established by Morris et al. (2002):

$$B = aD + bD^2 + c \quad (1)$$

where B is the vegetation biomass; D is the elevation; and a, b and c are coefficients that are determined by the vegetation type and location. Equation (1) has been used in many models to quantify the feedback between vegetation biomass and elevation (Fagherazzi et al., 2012; Twilley et al., 2019). The coefficients of vegetation types were determined by several typical vegetation species in a well-studied river-dominated delta (i.e., Wax Lake Delta), which mainly consists of freshwater marshes (Carle et al., 2014; Carle et al., 2015). The elevation range and biomass of each vegetation type were defined based on the mapped pixel-elevation histograms constructed by Carle et al. (2015), where the biomass remained zero at the lowest and highest elevation ranges and was largest at the median elevation range. Then, the values calculated in Equation (1) were used to solve the coefficients of each vegetation type (Table 3).

Table 2. Definitions of Modeling Scenarios

Scenarios	D_{50}(μm)	*COH* (m^3/s)	%Co
S1	30	0.20	77.50
S2	50	0.20	80.10
S3	100	0.00	0.00
S4	200	0.00	0.00
S5	300	0.00	0.00
S6	30	0.10	58.51
S7	30	0.09	49.69
S8	30	0.08	44.53
S9	30	0.05	36.67

**COH* is the concentration of cohesive sediment fraction; %Co is the percentage of cohesive sediment in the total sediment volume coming into the calculation domain.

The next step was the simulation of vegetation distribution on the delta based on the biomass-elevation curves (Figure 2). Essentially, the relationship between elevation and vegetation biomass is that elevation determines other environmental conditions and resources that support the survival of vegetation species by creating a wide range of potentially suitable niches for a wide variety of species (Damgaard et al., 2017; Twilley et al., 2019). Despite the effects of elevation, the distribution of vegetation is also affected by competition between different vegetation species (Chesson, 2000). The elevation-based niches of neighboring species overlap among different vegetation species, and the fitness determines the competitiveness of species (Chesson, 2000; Gallien et al., 2017). Niche fitness is the fundamental indicator that determines vegetation distribution and was defined in our research as the value of biomass, which could reflect the viability of certain species (Morris et al., 2002). Thus, to simulate the distribution of vegetation in the deltas, we retrieved bed-level elevation data from Delft3D at the end of each morphological run and calculated the biomass of each vegetation type based on Equation (1). The interspecific competition was simply simulated by comparing the value of biomass at niche overlapping areas. Finally, the distribution of vegetation was generally determined by the value of biomass, and the area was dominantly controlled by the species with the highest biomass (B) value.

Furthermore, we used landscape metrics to quantify the deltaic vegetation distribution pattern in each scenario. Landscape metrics are generally used for describing spatial heterogeneity, structure and composition of landscape covers, which has been widely used to quantify the spatial distribution patterns in coastal environments (Uuemaa et al., 2009; Wu et al., 2019). A patch is considered as the smallest element that makes up a landscape with homogenous conditions (Herold et al., 2005; Altamirano et al., 2010). In this study, patch boundaries were defined based on the connectivity of each type of vegetated grid to its eight neighboring grids (including four orthogonal and four diagonal neighbors) using the "bwlabel" function in MATLAB. Several commonly used landscape metrics were further calculated to quantify the spatial patterns of vegetation (Table 4). Patch density (PD) was used to indicate the fragmentation of vegetation distribution of the delta. The mean patch size (MPS) indicates the fragmentation of each vegetation type. The percentage of landscape (PLAND) represents the dominance of each vegetation type (Kumar et al., 2006; Uuemaa et al., 2009).

3. Results

As shown in Figure 3, the planform of delta morphology transformed from elongating along few channels to semicircular with many channels with increasing grain sizes (Figure 3), which is coincide with the results of previous studies (Edmonds and Slingerland, 2010; Geleynse et al., 2011; Caldwell and Edmonds, 2014). The results distinguished two vegetation distribution patterns between cohesive and noncohesive scenarios. With regard to the cohesive sediment scenarios, HEV was distributed mostly along the river channels, whereas SAV was generally located farther away from the channels (Figures 3a and 3b). In contrast, the transitional zone of HEV to SAV under the noncohesive sediment scenarios mainly ran from

Table 3. Vegetation Type, Representative Vegetation, Elevation Range, and Coefficients

Vegetation type	Representative vegetation	Elevation (m)	Coefficient *a*	Coefficient *b*	Coefficient *c*
HEV1	*Salix nigra*	0.40 ~ 0.98	1478.57	−1071.43	−420.00
MEV2	*Colocasia esculenta*	0.39 ~ 0.81	2721.09	−2267.57	−716.32
MEV1	*Polygonum spp.*	0.19 ~ 0.72	875.56	−1206.35	−165.03
SAV2	*Nelumbo lutea*	0.07 ~ 0.50	1292.00	−2266.67	−79.33
SAV1	*Elodea canadensis*	−0.18 ~ 0.45	207.27	−767.68	62.18

*SAV is submerged aquatic vegetation, MEV is mid-elevation vegetation and HEV is high-elevation vegetation

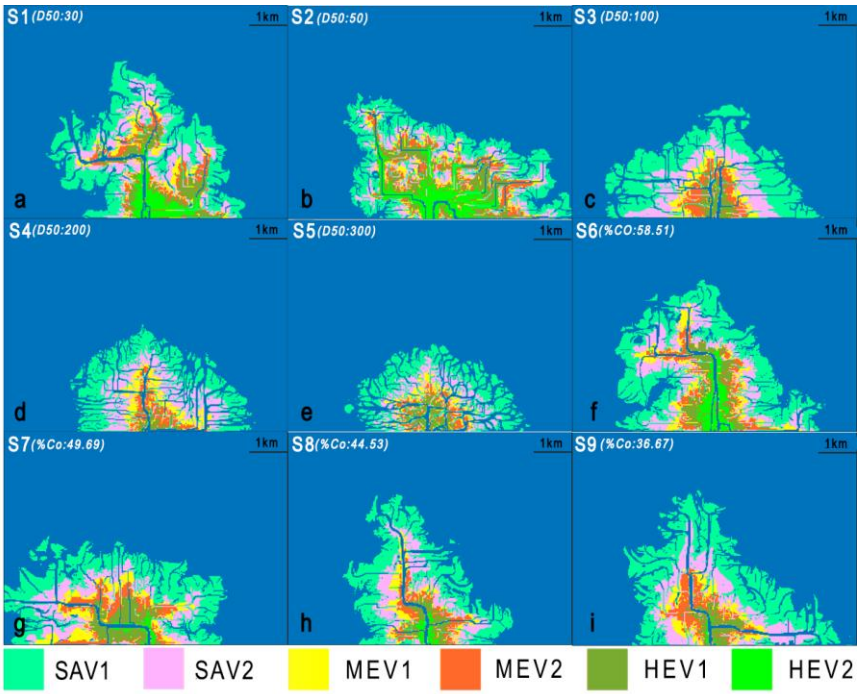

Figure 3. The simulated vegetation distribution patterns in different scenario. In cohesive scenarios (S1 ~ S2), HEV was distributed mostly along the river channels, whereas SAV was generally located farther away from the channels. The transitional zone of HEV to SAV under the noncohesive sediment scenarios (S3 ~ S5) mainly ran from the center to the edge of the delta.

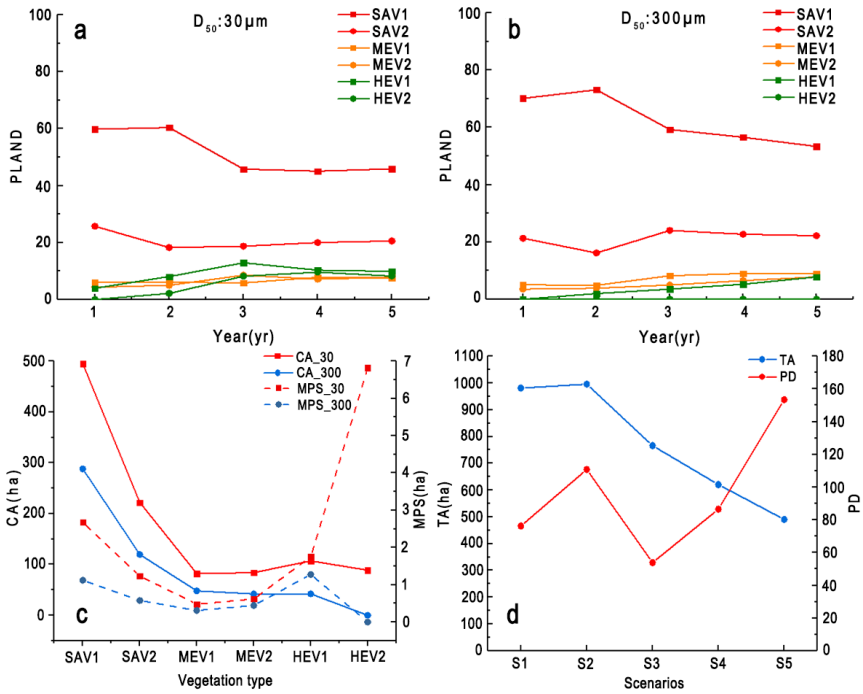

Figure 4. The PLAND indices of vegetation types in cohesive sediment scenario (S2) (a) and noncohesive sediment scenario (S6) (b). CA and MPS of vegetation types at the end of the simulation in scenarios S2 (*D*50: 30 μm) and S6 (*D*50: 300 μm) (c), the CA and MPS remain zero in scenario S6. TA and PD at landscape level at the end of the simulation in each scenario (d).

the center to the edge of the delta (Figures 3c ~ 3e). The differences in the vegetation distribution patterns of the cohesive and noncohesive deltas resulted from the varied deltaic elevation patterns, which were created by differential dominant delta-building processes between cohesive and noncohesive sediments.

Our results showed that the vegetation distribution pattern would become more like a noncohesive delta type when the ratio between cohesive and noncohensive sediments decreases (Figures 3f ~ 3i), which shows that the HEV would be more concentrated at the center of delta than it would be distributed along the channels. This phenomenon becomes notable when the sediments delivered into the delta are composed of a greater proportion of noncohesive sediments, even though the delta morphology in scenarios S8 and S9 presented elongated shapes, similar to those of cohesive deltas.

Here, we took scenarios S2 (D_{50}: 30 μm) and S6 (D_{50}: 300 μm) as two representative examples to illustrate the vegetation patterns since other scenarios basically show the same trends. In both scenarios, the PLAND of each vegetation type gradually became stable after the third morphological year of the simulation (Figures 4a and 4b), which indicates that the dominance of each vegetation type would gradually become stable when the delta grows mature. The comparison of MPS of different vegetation types showed that the MEV has the lowest MPS in both cohesive and noncohesive scenarios (Figure 4c), suggesting that the MEV exhibited a more fragmented distribution pattern compared with other vegetation types. At a delta landscape level, the PD remained middle values in cohesive scenarios and significantly increased with increasing grain sizes in noncohesive scenarios (Figure 4d). However, the difference in PD at the landscape level between cohesive scenarios and noncohesive scenarios might be attributed to the above-mentioned different distribution patterns between cohesive deltas and noncohesive deltas.

Table 4. Selected Landscape Metrics, Their Indicator Function, Metrics Levels and Equations

Landscape metrics	Indicator of	Level	Equation
Patch density (PD)	Fragmentation	Landscape	$PD = \frac{NP_d}{TA} \times 100$
Mean patch size (MPS)	Fragmentation	Class	$MPS = \frac{CA_I}{NP_I}$
Percentage of landscape (PLAND)	Dominance	Class	$PLAND = \frac{CA_I}{TA} \times 100$

*NP_d is the total number of patches on the delta; NP_I is the patch numbers of vegetation type; TA is the total vegetated area on the delta and CA_I is the area of vegetation type

4. Discussion

4.1. Comparison with Natural Delta

In this study, two distinct vegetation distribution patterns were formed with regard to cohesive and noncohesive deltas (Figure 3), which can be verified and demonstrated by two natural examples, i.e., the Yellow River Delta (YRD) in China and the Wax Lake Delta (WLD) in the United States of America, respectively. The two natural deltas that we selected are river-dominated deltas in which the measured marine energy is weak and the active morphological processes are primarily determined by river flow and the associated sediments (Galloway, 1975; Syvitski and Saito, 2007; Nienhuis et al., 2020).

As a typical river-dominated, cohesive delta with an average grain size of 24 μm (Syvitski and Saito, 2007; Yonggui et al., 2013), the YRD can be used as a natural example to verify our modeling results of the vegetation distribution pattern of cohesive deltas. Vegetation patterns have been well documented in the YRD and incorporate three major types, of which *Phragmites australis* is a perennial herbaceous species that dominates the upper tidal area, *Suaeda salsa* is a pioneer species that inhabits mudflats in the lower tidal area and *Spartina alterniflora* is an invasion plant that occupies the tidal zone (Gong et al., 2020; Ning et al., 2020). The vegetation type is generally transformed from *Phragmites australis* via *Suaeda salsa* to *Spartina alterniflora* when moving away from the river course in the vertical direction. In particular, the vegetation also showed the same distribution pattern around the Qingshuigou course, which has been abandoned since 1996 (Figure 5) (Syvitski and Saito, 2007). This vegetation pattern is notably consistent with our modeling results under the cohesive scenarios (Figure 3). Although salinity is regarded as another key factor affecting the vegetation pattern of the YRD (Fan et al., 2011), its regime and spatial pattern are also largely determined by its elevation pattern (Paola et al., 2011; White and Visser, 2016).

Sediment deposition in the WLD ranges from silt to sand (Shaw et al., 2014) of which sandy deposition is dominant at 67% and plays a key role in shaping the fan-like delta shape with many distributary channels (Roberts et al., 1997; Shaw et al., 2014). According to the vegetation classification maps of the WLD (Carle et al., 2014; Ma et al., 2018), woody vegetation (e.g., *Salix nigra*) mainly occurs at the upstream heads of islands, mixed grasses and forbs (such as *Colocasia esculenta* and *Polygonum spp.*) basically colonize the delta center, and submerged aquatic vegetation (such as *Nelumbo lutea* and *Potamogeton nodosus*) is mainly distributed at the delta's edge. In addition, silt deposition around the channel edges has generated a higher-elevation vegetation pattern along the channels (Carle et al., 2014). This center-to-edge vegetation pattern also generally follows what we observed under the noncohesive scenarios.

Deviated vegetation patterns also existed, particularly in both delta central areas, where the habitats were dominated by herbaceous vegetation, contrasting the woody vegetation obtained from the modeling results. This incongruence is probably because woody vegetation may take decades to grow under natural conditions even when the local environmental conditions are suitable.

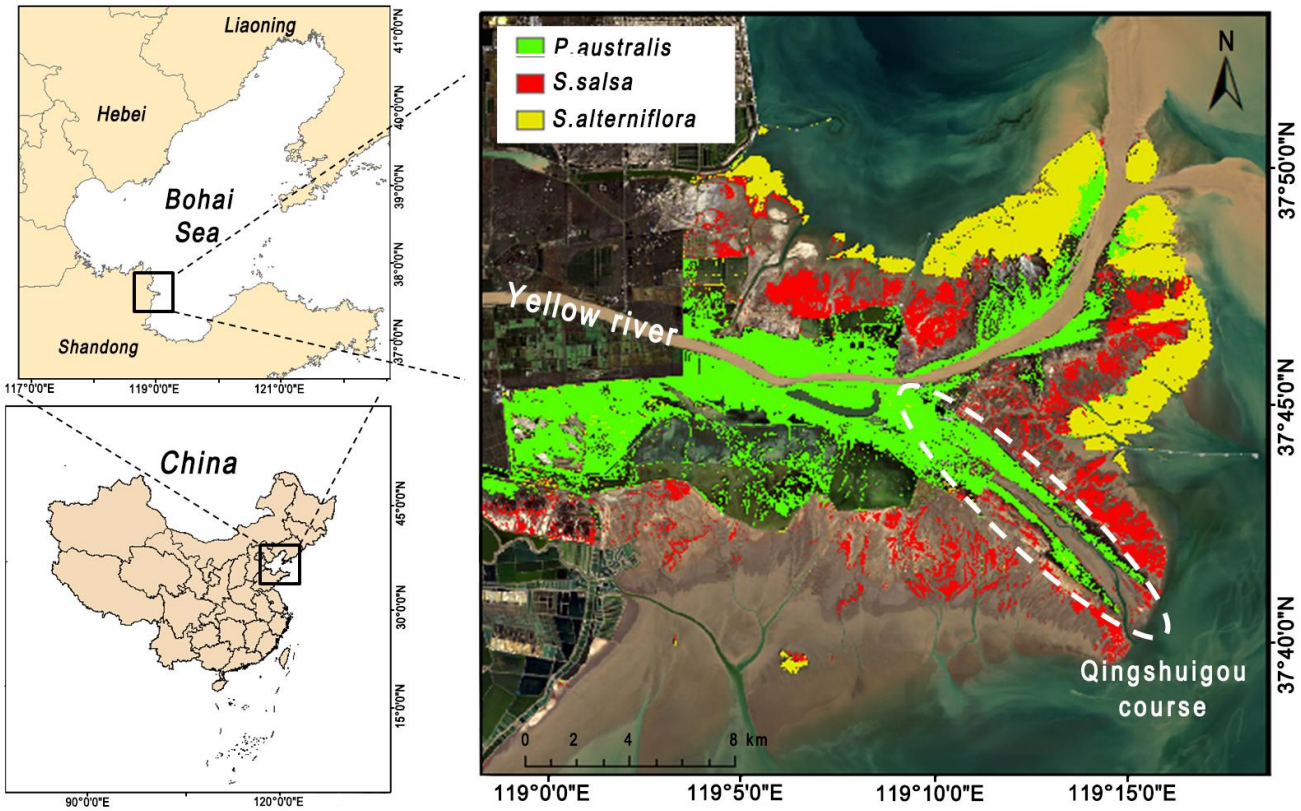

Figure 5. The YRD vegetation types were classified using remote sensing images in 2018. Modified from the vegetation classification maps of Gong et al. (2020).

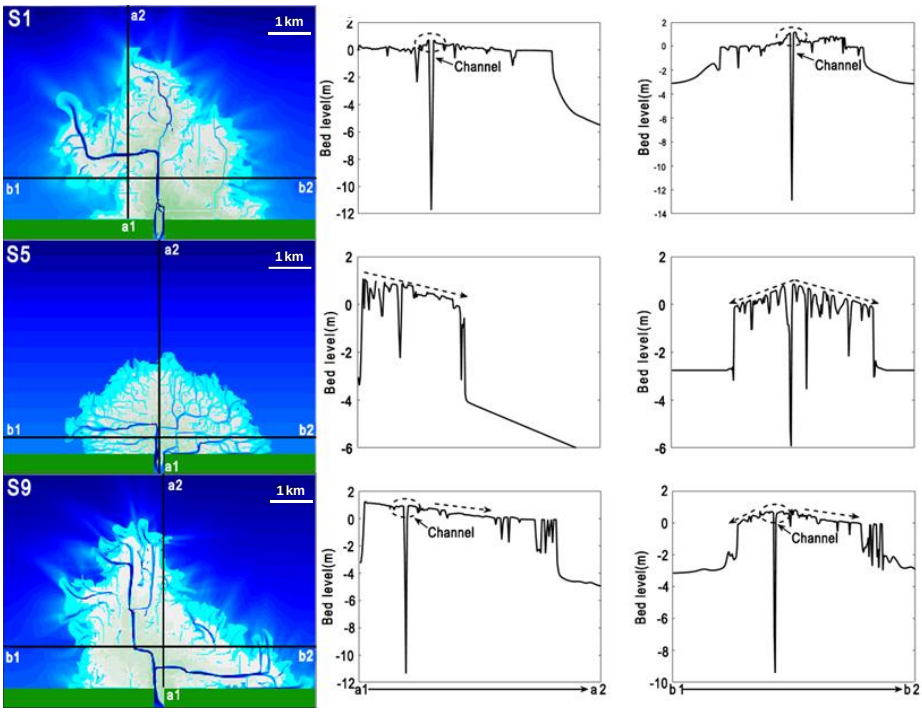

4.2. How Grain Size Determined Deltaic Vegetation Distribution Patterns

Although the vegetation distribution is known to be determined by multiple abiotic (i.e., water depth, salinity) and biotic (i.e., interspecific competition) factors (Edmonds and Slingerland, 2010; Burpee et al., 2015; Caldwell and Edmonds, 2014), our results indicated that grain size may substantially control the overall vegetation distribution pattern by governing the platform morphological features and processes of deltas. In addition, our results also confirmed that the vertical growth of deltas is the key factor that determines the distribution of vegetation species by affecting the overall habitat conditions within a delta (Bertness and Ellison, 1987; Paola et al., 2011; Carle et al., 2015). The elevation profiles of the cohesive (e.g., scenario S1) and noncohesive (e.g., scenario S5) deltas presented different patterns in our research. Under the cohesive scenarios, a higher elevation was observed near the channels, and the delta platform gradually flattened as it declined seaward, while the noncohesive delta sharply declined from the center to the edge area (Figure 6), congruent with the real elevation pattern of the WLD (Bevington et al., 2017). Following deltaic growth, a river bank with a higher elevation would create a suitable habitat for high-elevation adaptive vegetation and thus could create a distinct vegetation pattern along the channel in a cohesive delta, whereas high-elevation adapted vegetation would dominate the central area of non-cohesive deltas, and low-elevation adapted vegetation would occur at the edge of the delta due to its declined elevation.

Our results addressed the impacts of grain size on vertical delta landforms that affect the vegetation patterns of deltas. For example, coarse-grained, noncohesive sediment is deposited upstream of the jet plume with a rapid settling velocity compared with fine-grained, cohesive sediment transported to the ends of the jet due to a slow settling velocity. Cohesive sediments have a greater critical shear stress, which drives erosion, creating higher, more stable levees in cohesive deltas than in noncohesive deltas (Edmonds and Slingerland, 2010; Geleynse et al., 2011; Caldwell and Edmonds, 2014; Burpee et al., 2015). The higher concentration of cohesive sediments in fewer stable channels would constrain the deposition occurring near the channels through suspended transportation (Figure 7a) and facilitate the construction of high-elevation river banks (Hoyal et al., 2009b). Meanwhile, the smaller ratio between the width and depth of the stable channels (Figure 6) could create unstable turbulent jets at the channel mouth (Rowland et al., 2009; Canestrelli et al., 2014) and thus restrain the growth of the mouth bar but promote the lateral diffusivity of sediments, finally enhancing delta levee growth (Edmonds and Slingerland, 2010; Caldwell and Edmonds, 2014).

In contrast, noncohesive sediments would mostly aggregate at the river mouth or within the channels, leading to frequent channel avulsion and the formation of many mobile channels (Parker et al., 1998; Caldwell and Edmonds, 2014). In addition, bifurcations are produced following constant growth of the mouth bar and result in many distributary channels (McPherson et al., 1987). These two processes are frequently observed in noncohesive deltas and generate many channels and further create new land areas by delivering sediments to the delta's edges. When a noncohesive delta extends seawards, the older center area of the delta could still be fed by noncohesive sediment deposition through crevasses and thus maintain a higher elevation, while the newly emerged edge still remains lower (Figure 7b). This chronosequential pattern can be well exemplified by the morphological dynamics of the WLD (Bevington et al., 2018).

Furthermore, our results demonstrated that the ratio between cohesive and noncohesive sediments determines the resulting vegetation pattern through its impact on elevation patterns in deltas (Figure 3). For example, although the elevation of a noncohesive sediment-dominated delta (scenario S9) declines from the center to the edge of the delta (Figure 6) and further shapes the corresponding vegetation patterns, unstable turbulent jets are created at the river mouth due to the presence of partially added cohesive sediments that promote the formation of channels with a smaller ratio between their widths to depths (Figure 6). Unstable turbulent jets reduce potential avulsion and prolong the running time of channels (Caldwell and Edmonds, 2014). However, noncohesive sediments may facilitate the growth of river mouth bars and bifurcations with shorter transportation and deposition distances (Edmonds and Slingerland, 2007; Kleinhans et al., 2008). In our results, the bifurcated channels were not very stable, and one of the bifurcated channels was gradually abandoned and filled with sediments due to the decreased water flow. This process was consistent with the findings of Hoyal et al. (2009a) and Edmonds and Slingerland, (2010) in cohesive deltas. Meanwhile, levees mainly composed of noncohesive dominated sediments would also be unstable compared with those formed with cohesive dominated sediments, and overbank flow would be produced within the channels and create incisions around the main channel when the aggradation effects are stronger than unstable turbulent jets at channel mouth (Figure 7c). These temporary incisions could deliver sediments onto the adjacent shorelines around the overall delta edges. In all, on one hand, the delta would prograde with main channels due to erosive unstable turbulent jet, on the other hand, the frequent overbank flow formed incisions can transport sediment into the delta edge. These two main processes could distribute massive noncohesive sediments to the delta perimeter and finally show elevation patterns more like noncohesive sediments constructed deltas.

Our research indicates that cohesive and noncohesive sediments could jointly control the morphological evolution of a delta and further affect its vegetation distribution pattern, which can also be observed in the WLD. Although this sand-dominated (i.e., noncohesive sediments) delta has a fan-like shape with many distributary channels, a considerable amount of silt (cohesive sediments) may be deposited at the channel edges and help stabilize these bifurcation channels while increasing delta elevation (Shaw et al., 2013b; Bevington et al., 2017). Under natural conditions, sediments are always composed of a wide range of sediment grain sizes, and these sediment depositional dynamics may collectively affect delta morphological evolution processes simultaneously. However, the impacts of major sediment components should be captured and highlighted, as

they play a key role in building the resulting delta morphology and further determining vegetation distribution patterns.

4.3. The Factors that Affect Deltaic Vegetation Patterns

The river discharge carried sediments into the receiving basin, which promoted the significant growth of the delta and led to each vegetation species taking a stable proportion as delta grows mature (Figures 4a and 4b). In an active river-dominated delta, the river discharges and associated sediment yields are the main factors that control topography of deltaic floodplain, controlling the vegetation patterns (Rosen and Xu, 2013; Carle et al., 2015; Ma et al., 2018). The net input of sediments leads to the progradation of the delta and causes the accretion of elevation. The newly formed lands could provide a platform for more vegetation colonized on the delta (Paola et al., 2011; Rosen and Xu, 2013) and the increase in elevation creates more suitable environmental conditions for high-elevation vegetation, which improves the proportion of high-elevation as delta prograding (Carle et al., 2015; Ma et al., 2018). Meanwhile, the competition between vegetation species in niches-overlapping areas can cause vegetation to be restricted in the area with the highest fitness, resulting in vegetation occupying the most suitable elevations and taking a stable proportion as the delta grows mature.

Our results also showed that the MEV presented with a more fragmented pattern than other vegetation types (Figure 4c). Here, we illustrate the vegetation succession processes on one delta lobe in scenario S3 at the end of each morphological year. As shown in Figure 8, the MEV was gradually cut into more small patches as delta prograding. This process could be interpreted by the competition between vegetation species. At first, the mid-elevation vegetation dominated the area with few large patches; however, the fitness of the high-elevation vegetation increased while the mid-elevation vegetation gradually lost their fitness due to the constant increase in the elevation with the prograding delta, which implies that the mid-elevation vegetation lost its competitive with high-elevation vegetation and the area gradually converted into high-elevation vegetation. Meanwhile, the expansion of the mid-elevation vegetation was also limited by the low-elevation vegetation, resulting in the distribution of the mid-elevation vegetation present with many small patches as the delta grows to mature. This also indicates that the landform as the initial environmental factor determines the vegetation distribution patterns of the entire delta, but the distribution pattern of each vegetation type may be affected by various processes, such as environmental factors and interspecies competition at the same time (Shaffer et al., 1992).

4.4. Model Limitation

In our study, the vegetation patterns were modeled and identified by only considering the tolerance of individual species to elevation patterns and their interactive competition in areas where their niches overlapped. We did not incorporate the bidirectional eco-geomorphic feedback between vegetation and landform types into our modeling research due to a lack of field surveys and site-based data. Although the sediment supply and its grain size are regarded as the key factors controlling delta morphology and vegetation distribution patterns (Carle et al., 2015; Lokhorst et al., 2018), the lack of consideration for the ecogeomorphic feedback between vegetation and elevation may lead to the underestimation of elevation gains on delta and channel stabilization, particularly in intermediate elevation zones where ecogeomorphic feedback between vegetation and Elevation is prominent. In addition, the effects of different vegetation communities also need to be considered in future research, as they could function in different roles in deltaic landscape evolution (Ma et al., 2018).

5. Conclusions

In this research, we conducted numerical experiments using Delft3D to simulate deltaic morphological evolution and vegetation distribution patterns in response to sediment grain sizes. The results indicate that transformation from high-elevation to low-elevation adaptive vegetation species would occur from the river banks to the shoreline of cohesive deltas with fine-grained sediments, compared with the same transformation observed from center to edge in noncohesive deltas with large-grained sediments. The two simulated vegetation distribution patterns are consistent with those in natural deltas, such as the Yellow River Delta and the Wax Lake Delta.

Fine-grained cohesive sediments could build firm levees with stable channels, and a high concentration of cohesive sediments would create a suitable habitat for high-elevation adapted vegetation by accelerated deposition around the channels. Large-grained, noncohesive sediments would result in frequent avulsion and form many mobile channels, and the sediments constantly transported to delta peripheries through these channels and deposited in numerous crevasses would maintain high- er elevations in older centers and lower elevations at the new edges of a delta. The morphological processes would be controlled by both cohesive versus noncohesive sediments, and the sediment with the largest proportion would dominantly control the vegetation distribution patterns by shaping delta elevation patterns.

The dominance of high-elevation vegetation is gradually increasing with the decrease in low-elevation vegetation and the proportion of vegetation types gradually holds stable as the delta grows mature. Meanwhile, the expansion of high-elevation vegetation and the limitation of low-elevation vegetation could result in a more fragmented pattern of mid-elevation vegetation. This theoretical and templet-based study explored and discussed the effects of sediment grain size on the deltaic vegetation distribution patterns associated with morphological processes, which may have potential general implications for the conservation and restoration of deltaic habitats; however, the reality-based quantitative research should be conducted in future.

Acknowledgements. This work was supported by the National Key R&D Program of China (Grant 2019YFE0121500), the Joint Funds

of the National Natural Science Foundation of China (U22A20558，U2006215) and the National Natural Science Foundation of China (No. 32171572 & 31770576).

References

Altamirano, J.P., Primavera, J.H., Banaticla, M.R.N. and Kurokura, H. (2010). Practical techniques for mapping small patches of mangroves. *Wetl. Ecol. Manage*., 18(6), 707-715. https://doi.org/10.1007/s11273-010-9190-2

Barbier, E.B., Hacker, S.D., Kennedy, C., Koch, E.W., Stier, A.C. and Silliman, B.R. (2011). The value of estuarine and coastal ecosystem services. *Ecol. Monogr*., 81(2), 169-193. https://doi.org/10.1890/10-1510.1

Bertness, M.D. and Ellison, A.M. (1987). Determinants of pattern in a new england salt marsh plant community. *Ecol. Monogr.*, 57(2), 129-147. https://doi.org/10.2307/1942621

Bevington, A.E. and Twilley, R.R. (2018). Island edge morphodynamics along a chronosequence in a prograding deltaic floodplain wetland. *J. Coast. Res*., 34(4), 806-817. https://doi.org/10.212/jcoastres-d-17-00074.1

Bevington, A.E., Twilley, R.R., Sasser, C.E. and Holm, G.O. (2017). Contribution of river floods, hurricanes, and cold fronts to elevation change in a deltaic floodplain, northern Gulf of Mexico, USA. *Estuar. Coast. Shelf Sci*., 191, 188-200. https://doi.org/10.1016/j.ec ss.2017.04.010

Burpee, A.P., Slingerland, R.L., Edmonds, D.A., Parsons, D., Best, J., Cederberg, J., McGuffin, A., Caldwell, R., Nijhuis, A. and Royce, J. (2015). Grain-size controls on the morphology and internal geometry of river-dominated deltas. *J. Sediment. Res*., 85(6), 699-714. https://doi.org/10.2110/jsr.2015.39

Caldwell, R.L. and Edmonds, D.A. (2014). The effects of sediment properties on deltaic processes and morphologies: A numerical modeling study. *J. Geophys. Res. Earth Surf*., 119(5), 961-982. https://doi.org/10.1002/2013jf002965

Canestrelli, A., Nardin, W., Edmonds, D., Fagherazzi, S. and Slingerland, R. (2014). Importance of frictional effects and jet instability on the morphodynamics of river mouth bars and levees. *J. Geophys. Res. Oceans*, 119(1), 509-522. https://doi.org/10.1002/2013 JC009312

Carle, M.V., Sasser, C.E. and Roberts, H.H. (2015). Accretion and vegetation community change in the Wax Lake Delta following the historic 2011 Mississippi River flood. *J. Coast. Res*., 31(3), 569-587. https://doi.org/10.2112/jcoastres-d-13-00109.1

Carle, M.V., Wang, L. and Sasser, C.E. (2014). Mapping freshwater marsh species distributions using WorldView-2 high-resolution multispectral satellite imagery. *Int. J. Remote Sens*., 35(13), 4698-4716. https://doi.org/10.1080/01431161.2014.919685

Chesson, P. (2000). Mechanisms of maintenance of species diversity. *Annu. Rev. Ecol. Syst*., 31(1), 343-366. https://doi.org/10.1146/annurev.ecolsys.31.1.343

Damgaard, C., Merlin, A. and Bonis, A. (2017). Plant colonization and survival along a hydrological gradient: demography and niche dynamics. *Oecologia*, 183(1), 201-210. https://doi.org/10.1007/s00442-016-3760-9

Deltares (2013). *Delft3D-Flow: Simulation of Multi-Dimensional Hydrodynaminc Flows and Transport Phenomena, Including Sediments*. User Manual. Delft, Netherlands: Deltares, 614.

Edmonds, D.A. and Slingerland, R.L. (2007). Mechanics of river mouth bar formation: Implications for the morphodynamics of delta distributary networks. *J. Geophys. Res. Earth Surf*., 112(F2), 1-14. https://doi.org/10.1029/2006jf000574

Edmonds, D.A. and Slingerland, R.L. (2010). Significant effect of sediment cohesion on delta morphology. *Nat. Geosci*., 3(2), 105-109. https://doi.org/10.1038/ngeo730

Fagherazzi, S., Kirwan, M.L., Mudd, S.M., Guntenspergen, G.R., Temmerman, S., D'Alpaos, A., van de Koppel, J., Rybczyk, J.M., Reyes, E., Craft, C. and Clough, J. (2012). Numerical models of salt marsh evolution: Ecological, geomorphic, and climatic factors. *Rev. Geophys*., 50(1), 1-28. https://doi.org/10.1029/2011rg000359

Fan, X., Pedroli, B., Liu, G., Liu, H., Song, C. and Shu, L. (2011). Potential plant species distribution in the Yellow River Delta under the influence of groundwater level and soil salinity. *Ecohydrol*., 4(6), 744-756. https://doi.org/10.1002/eco.164

Gallien, L., Zimmermann, N.E., Levine, J.M. and Adler, P.B. (2017). The effects of intransitive competition on coexistence. *Ecol. Lett*., 20(7), 791-800. https://doi.org/10.1111/ele.12775

Galloway, W.E. (1975). *Process Framework for Describing the Morphologic and Stratigraphic Evolution of Deltaic Depositional System.* Society of Economic Paleontologists and Mineralogist, Special Publication No 31, 127-156.

Gao, W., Shao, D., Wang, Z.B., Nardin, W., Rajput, P., Yang, W., Sun, T. and Cui, B. (2019). Long-term cumulative effects of intra-annual variability of unsteady river discharge on the progradation of delta lobes: A modeling perspective. *J. Geophys. Res. Earth Surf*., 124(4), 960-973. https://doi.org/10.1029/2017JF004584

Gao, W., Shao, D., Wang, Z.B., Nardin, W., Yang, W., Sun, T. and Cui, B. (2018). Combined effects of unsteady river discharges and wave conditions on river mouth bar morphodynamics. *Geophys. Res. Lett*., 45(23), 12903-12911. https://doi.org/10.1029/2018gl08 0447

Geleynse, N., Storms, J.E.A., Stive, M.J.F., Jagers, H.R.A. and Walstra, D.J.R. (2010). Modeling of a mixed-load fluvio-deltaic system. *Geophys. Res. Lett*., 37(5), L05402. https://doi.org/10.1029/2009gl042000

Geleynse, N., Storms, J.E.A., Walstra, D.-J.R., Jagers, H.R.A., Wang, Z.B. and Stive, M.J.F. (2011). Controls on river delta formation; insights from numerical modelling. *Earth Planet. Sci. Lett*., 302 (1-2), 217-226. https://doi.org/10.1016/j.epsl.2010.12.013

Gong, Z., Zhang, C., Zhang, L., Bai, J. and Zhou, D. (2020). Assessing spatiotemporal characteristics of native and invasive species with multi-temporal remote sensing images in the Yellow River Delta, China. *Land Degrad. Dev.*, 32(3), 1338-1352. https://doi.org/10.1002/ldr.3799

Herold, M., Couclelis, H. and Clarke, K.C. (2005). The role of spatial metrics in the analysis and modeling of urban land use change. *Comput. Environ. Urban Syst*., 29(4), 369-399. https://doi.org/10.1016/j.compenvurbsys.2003.12.001

Hoyal, D.C.J.D. and Sheets, B.A. (2009). Morphodynamic evolution of experimental cohesive deltas. *J. Geophys. Res. Earth Surf*., 114 (F2), 1-18. https://doi.org/10.1029/2007JF000882

Ikeda, S. (1982). Incipient motion of sand particles on side slopes. *J. Hydraul. Div*., 108(1), 95-114. https://doi.org/10.1061/JYCEAJ.0005812

Kleinhans, M.G., Jagers, H.R.A., Mosselman, E. and Sloff, C.J. (2008). Bifurcation dynamics and avulsion duration in meandering rivers by one-dimensional and three-dimensional models. *Water Resour. Res*., 44(8), 1-31. https://doi.org/10.1029/2007WR005912

Kumar, S., Stohlgren, T.J. and Chong, G.W. (2006). Spatial heterogeneity influences native and nonnative plant species richness. *Ecology*, 87(12), 3186-3199. https://doi.org/10.1890/0012-9658(2006)87[3186:SHINAN]2.0.CO;2

Larsen, L.G. (2019). Multiscale flow-vegetation-sediment feedbacks in low-gradient landscapes. *Geomorphology*, 334, 165-193. https://doi.org/10.1016/j.geomorph.2019.03.009

Lauzon, R. and Murray, A.B. (2018). Comparing the cohesive effects of mud and vegetation on delta evolution. *Geophys. Res. Lett*., 45 (19), 10437-10445. https://doi.org/10.1029/2018gl079405

Liviu, G., James, S., Stefan, C. and John, D. (2014). Climate change: Protect the world's deltas. *Nature*, 516(7529), 31-33. https://doi.org/10.1038/516031a

Lokhorst, I.R., Braat, L., Leuven, J.R.F.W., Baar, A.W., van Oorschot, M., Selaković, S. and Kleinhans, M.G. (2018). Morphological ef-

fects of vegetation on the tidal–fluvial transition in Holocene estuaries. *Earth Surf. Dyn*., 6(4), 883-901. https://doi.org/10.5194/esurf-6-883-2018

Ma, H., Larsen, L.G. and Wagner, R.W. (2018). Ecogeomorphic feed -backs that grow deltas. *J. Geophys. Res. Earth Surf*., 123(12), 3228-3250. https://doi.org/10.1029/2018jf004706

Ma, T., Li, X., Bai, J. and Cui, B. (2019). Tracking three decades of land use and land cover transformation trajectories in China's large river deltas. *Land Degrad. Dev*., 30(7), 799-810. https://doi.org/10.1002/ldr.3268

McPherson, J.G., Shanmugam, G. and Moiola, R.J. (1987). Fan-deltas and braid deltas: Varieties of coarse-grained deltas. *Geol. Soc. Am. Bull*., 99(3), 331-340. https://doi.org/10.1130/0016-7606

Morris, J.T., Sundareshwar, P.V., Nietch, C.T., Kjerfve, B. and Cahoon, D.R. (2002). Responses of coastal wetlands to rising sea level. *Ecology*, 83(10), 2869-2877. https://doi.org/10.1890/0012-9 658

Nienhuis, J.H., Ashton, A.D., Edmonds, D.A., Hoitink, A.J.F., Kettner, A.J., Rowland, J.C. and Tornqvist, T.E. (2020). Global-scale human impact on delta morphology has led to net land area gain. *Nature*, 577(7791), 514-518. https://doi.org/10.1038/s41586-019-1905-9

Ning, Z., Chen, C., Xie, T., Wang, Q., Bai, J., Shao, D., Man, Y. and Cui, B. (2020). Windows of opportunity for smooth cordgrass landward invasion to tidal channel margins: The importance of hydrodynamic disturbance to seedling establishment. *J. Environ. Manage*., 266, 110559. https://doi.org/10.1016/j.jenvman.2020.110559

Ning, Z., Chen, C., Zhu, Z., Xie, T., Wang, Q., Cui, B. and Bouma, T.J. (2021). Tidal channel-mediated gradients facilitate Spartina alterniflora invasion in coastal ecosystems: implications for invasive species management. *Mar. Ecol. Prog. Ser*., 659, 59-73. https://doi.org/10.3354/meps13560

Paola, C., Twilley, R.R., Edmonds, D.A., Kim, W., Mohrig, D., Parker, G., Viparelli, E. and Voller, V.R. (2011). Natural processes in delta restoration: application to the Mississippi Delta. *Ann. Rev. Mar. Sci*., 3, 67-91. https://doi.org/10.1146/annurev-marine-120709-142856

Parker, G. and Paola, C. (1998). Alluvial fans formed by channelized fluvial and sheet flow. I: Theory. *J. Hydraul. Eng*., 124(10), 985. https://doi.org/10.1061/(ASCE)0733-9429(1998)124:10(985)

Partheniades, E. (1965). Erosion and deposition of cohesive soils. *J. Hydraul. Div*., 91(1), 105-139. https://doi.org/10.1061/JYCEAJ.0001165

Roberts, H., Walker, N., Cunningham, R., Kemp, G.P. and Majersky, S. (1997). Evolution of sedimentary architecture and surface morphology: Atchafalaya and Wax Lake Deltas, Louisiana (1973-1994). *GCAGS Transactions*, 47, 477-484.

Rosen, T. and Xu, Y.J. (2013). Recent decadal growth of the Atchafalaya River Delta complex: Effects of variable riverine sediment input and vegetation succession. *Geomorphology*, 194, 108-120. https://doi.org/10.1016/j.geomorph.2013.04.020

Rowland, J.C., Stacey, M.T. and Dietrich, W.E. (2009). Turbulent characteristics of a shallow wall-bounded plane jet: experimental implications for river mouth hydrodynamics. *J. Fluid. Mech*., 627, 423-449. https://doi.org/10.1017/S0022112009006107

Shaffer, G.P., Sasser, C.E., Gosselink, J.G. and Rejmanek, M. (1992). Vegetation dynamics in the emerging atchafalaya delta, Louisiana, USA. *J. Ecol*., 80(4), 677-687. https://doi.org/10.2307/2260859

Shaw, J.B. and Mohrig, D. (2014). The importance of erosion in distributary channel network growth, Wax Lake Delta, Louisiana, USA. *Geology*, 42(1), 31-34. https://doi.org/10.1130/g34751.1

Shaw, J.B., Mohrig, D. and Whitman, S.K. (2013). The morphology and evolution of channels on the Wax Lake Delta, Louisiana, USA. *J. Geophys. Res. Earth Surf*., 118(3), 1562-1584. https://doi.org/10.1002/jgrf.20123

Syvitski, J.P.M. and Saito, Y. (2007). Morphodynamics of deltas under the influence of humans. *Global Planet. Change*, 57(3-4), 261-282. https://doi.org/10.1016/j.gloplacha.2006.12.001

Twilley, R.R., Day, J.W., Bevington, A.E., Castaiieda-Moya, E., Christensen, A., Holm, G., Heffner, L.R., Lane, R., McCall, A., Aarons, A., Li, S., Freeman, A. and Rovai, A.S. (2019). Ecogeomorphology of coastal deltaic floodplains and estuaries in an active delta: Insights from the Atchafalaya Coastal Basin. *Estuar. Coast. Shelf Sci*., 227, 106341. https://doi.org/10.1016/j.ecss.2019.106341

Uuemaa, E., Antrop, M., Roosaare, J., Marja, R. and Mander, Ü. (2009). Landscape metrics and indices: An overview of their use in landscape research. *Liv. Rev. Landscap. Res*., 3(1), 1-28. https://doi.org/10.12942/lrlr-2009-1

Van Rijn, L.C. (1993). *Principles of Sediment Transport in Rivers, Estuaries and Coastal Seas*. Amsterdam: Aqua publications.

White, D.A. and Visser, J.M. (2016). Water quality change in the Mississippi River, including a warming river, explains decades of wetland plant biomass change within its Balize delta. *Aquat. Bot*., 132, 5-11. https://doi.org/10.1016/j.aquabot.2016.02.007

Wilcox, D.A. (2004). Implications of hydrologic variability on the succession of plants in Great Lakes wetlands. *Aquat. Ecosyst. Health Manage.*, 7(2), 223-231. https://doi.org/10.1080/14634980 490461579

Wu, M., Li, C., Du, J., He, P., Zhong, S., Wu, P., Lu, H. and Fang, S. (2019). Quantifying the dynamics and driving forces of the coastal wetland landscape of the Yangtze River Estuary since the 1960s. *Reg. Stud. Mar. Sci*., 32, 100854. https://doi.org/10.1016/j.rsma.2019.100854

Yu, Y., Shi, X., Wang, H., Yue, C., Chen, S., Liu, Y., Hu, L. and Qiao, S. (2013). Effects of dams on water and sediment delivery to the sea by the Huanghe (Yellow River): The special role of Water-Sediment Modulation. *Anthropocene*, 3, 72-82. https://doi.org/10.1016/j.ancene.2014.03.001